

# Fermi polaron-polaritons in charge-tunable atomically thin semiconductors

Meinrad Sidler<sup>1\*</sup>, Patrick Back<sup>1</sup>, Ovidiu Cotlet<sup>1</sup>, Ajit Srivastava<sup>2</sup>, Thomas Fink<sup>1</sup>, Martin Kroner<sup>1</sup>, Eugene Demler<sup>3</sup> and Atac Imamoglu<sup>1\*</sup>

**The dynamics of a mobile quantum impurity in a degenerate Fermi system is a fundamental problem in many-body physics. The interest in this field has been renewed due to recent ground-breaking experiments with ultracold Fermi gases<sup>1–5</sup>. Optical creation of an exciton or a polariton in a two-dimensional electron system embedded in a microcavity constitutes a new frontier for this field due to an interplay between cavity coupling favouring ultralow-mass polariton formation<sup>6</sup> and exciton–electron interactions leading to polaron or trion formation<sup>7,8</sup>. Here, we present cavity spectroscopy of gate-tunable monolayer MoSe<sub>2</sub> (ref. 9) exhibiting strongly bound trion and polaron resonances, as well as non-perturbative coupling to a single microcavity mode<sup>10,11</sup>. As the electron density is increased, the oscillator strength determined from the polariton splitting is gradually transferred from the higher-energy repulsive exciton-polaron resonance to the lower-energy attractive exciton-polaron state. Simultaneous observation of polariton formation in both attractive and repulsive branches indicates a new regime of polaron physics where the polariton impurity mass can be much smaller than that of the electrons. Our findings shed new light on optical response of semiconductors in the presence of free carriers by identifying the Fermi polaron nature of excitonic resonances and constitute a first step in investigation of a new class of degenerate Bose–Fermi mixtures<sup>12,13</sup>.**

Transition metal dichalcogenide (TMD) monolayers represent a new class of two-dimensional (2D) semiconductors exhibiting features such as strong Coulomb interactions<sup>14</sup>, locking of spin and valley degrees of freedom due to large spin–orbit coupling<sup>9</sup> and finite electron/exciton Berry curvature with novel transport and optical signatures<sup>15,16</sup>. Unlike quantum wells or 2D electron systems (2DES) in III–V semiconductors, TMD monolayers exhibit an ultralarge exciton binding energy  $E_{\text{exc}}$  of order 0.5 eV (ref. 14) and strong trion peaks in photoluminescence (PL) that are redshifted from the exciton line by  $E_{\text{T}} \sim 30$  meV (refs 9,17). These features provide a unique opportunity to investigate many-body physics associated with trion<sup>18</sup> formation as well as coupling of excitons to a 2DES<sup>19</sup> and to cavity photons<sup>20,21</sup>, provided that the experimental set-up allows for varying the electron density  $n_e$  and light–matter coupling strength  $g_c$ .

Here, we carry out an investigation of Fermi polarons<sup>1</sup> in a charge-tunable MoSe<sub>2</sub> monolayer embedded in an open microcavity structure (Fig. 1a,b). Since  $E_{\text{exc}}$  is much larger than all other relevant energy scales, such as the normal mode splitting ( $2g_c$ ),  $E_{\text{T}}$  and the Fermi energy ( $E_{\text{F}}$ ), an optically generated exciton in a TMD monolayer can be considered as a robust mobile bosonic impurity

embedded in a fermionic reservoir (Fig. 1c). The Hamiltonian describing the system is

$$H = \omega_c c_0^\dagger c_0 + \sum_k \omega_X(k) x_k^\dagger x_k + g_c (c_0^\dagger x_0 + \text{h.c.}) + \sum_k \epsilon_k e_k^\dagger e_k + \sum_{k,k',q} V_q (x_{k+q}^\dagger e_{k'-q}^\dagger e_{k'} x_k + \text{h.c.}) \quad (1)$$

where the first line describes the coupling of 2D excitons, described by the exciton annihilation operator  $x_k$  to a 0D cavity mode  $c_0$  whose resonance frequency  $\omega_c$  can be tuned by applying a voltage ( $u_p$ ) to a piezoelectric actuator that changes the cavity length. This part of the Hamiltonian corresponds to the elementary building block of the recent ground-breaking experiments based on coupled 0D-polariton systems<sup>22</sup>. The second line of the Hamiltonian describes the Feshbach-like physics associated with the bound-molecular (trion) channel and the corresponding effective interactions between the excitons and the electrons<sup>1</sup>. This simplified description is valid in the low  $n_e$  limit where the inter-electron separation is much larger than the exciton Bohr radius  $a_B$  and consequently the exciton can be treated as a rigid impurity in a 2DES. We note that a similar approach was recently used to describe optical excitations in modulation doped II–VI semiconductor quantum wells<sup>23,24</sup>. To take into account the exciton energy blueshift ( $\delta(E_{\text{F}})$ ) due to the combined effects of phase space filling, screening and bandgap renormalization, we choose the exciton dispersion as  $\omega_X(k) = -E_{\text{exc}} + \delta(E_{\text{F}}) + k^2/2m_{\text{exc}}$ , where  $\delta(E_{\text{F}}) = \beta E_{\text{F}}$  and  $\beta$  is a fitting parameter (see Supplementary Information). We remark that the key polaronic features we explore here are independent of  $\delta(E_{\text{F}})$ .

The Fermi polaron problem describes the screening of a mobile impurity via generation of particle–hole pairs across the Fermi surface (Fig. 1c). When the impurity is a fermion with different spin, this problem corresponds to the highly polarized limit of a strongly interacting Fermi system<sup>1</sup>. The corresponding systems exhibit a wealth of complex phenomena, such as the elusive Fulde–Ferrell–Larkin–Ovchinnikov pairing mechanism, the Chandrasekhar–Clogston limit of BCS superconductivity and itinerant ferromagnetism<sup>25</sup>. While the cavity spectroscopy we implement to study the exciton–2DES problem in the weak-coupling regime is analogous to the radiofrequency spectroscopy of impurities in degenerate Fermi gases<sup>2</sup>, the strong-coupling regime of the TMD-monolayer–microcavity system represents a new frontier for quantum impurity physics. More specifically, since the exciton-polariton dispersion can be tuned by changing  $\omega_c(u_p) - E_{\text{exc}}$  to yield an effective polariton mass that is (up to) four orders of magnitude

<sup>1</sup>Institute of Quantum Electronics, ETH Zürich, CH-8093 Zürich, Switzerland. <sup>2</sup>Physics Department, Emory University, Atlanta, Georgia 22138, USA.

<sup>3</sup>Physics Department, Harvard University, Cambridge, Massachusetts 02138, USA. \*e-mail: sidlerme@phys.ethz.ch; imamoglu@phys.ethz.ch

smaller than that of the electron<sup>6</sup>, the extension of our experiments to a 2D cavity could realize a Fermi-polaron system with a tunable ultrasmall mass impurity.

We embed a MoSe<sub>2</sub>/hBN/graphene heterostructure<sup>26</sup> inside an open optical cavity<sup>27</sup> consisting of a flat dielectric mirror and a fibre mirror with a radius of curvature of 30  $\mu\text{m}$  (Fig. 1a). We use the graphene layer as a top gate that controls the electron density in the MoSe<sub>2</sub> layer (Fig. 1b), allowing us to tune the Fermi energy from  $E_F = 0$  to  $E_F \geq E_T$ , or equivalently, from  $n_e = 0$  to  $n_e \geq 5 \times 10^{12} \text{ cm}^{-2}$ . The thickness of the hBN layer is chosen to ensure that the MoSe<sub>2</sub> is located at an antinode of the cavity, while the graphene monolayer is at a node where the intra-cavity field vanishes; this choice ensures that the graphene absorption does not lead to a deterioration of the cavity finesse, which we estimate to be  $\mathcal{F} \sim 200$ .

To characterize the elementary optical excitations of the MoSe<sub>2</sub> monolayer, we set the cavity length to  $L_{\text{cav}} = 9.1 \mu\text{m}$ , and the sample temperature to  $T = 4 \text{ K}$ , and carry out spectroscopy in the limit of weak (perturbative) coupling to the cavity mode. Figure 2a depicts the cavity transmission spectrum in this weak-coupling regime obtained for  $V_g = -3 \text{ V}$ : the parallel diagonal lines correspond to transmission maxima associated with neighbouring axial modes of the cavity. Zooming in to the central mode, we find that the mode energy as well as its linewidth varies non-trivially due to coupling to the MoSe<sub>2</sub> excitations. We plot the colour-coded cavity line broadening (Fig. 2b) and line shift (Fig. 2c) as a function of  $V_g$  (vertical axis) and the fundamental cavity mode frequency (horizontal axis). Since the bare cavity linewidth ( $\sim 0.38 \text{ meV}$ ) is much smaller than the spectral features associated with excitonic resonances, the increase in cavity linewidth, or shift in cavity resonance frequency allows us to determine the imaginary (absorption) and real (dispersion) parts of MoSe<sub>2</sub> linear susceptibility (Fig. 2b,c). We note that even for  $L_{\text{cav}} = 9.1 \mu\text{m}$ , the exciton resonance is in the strong-coupling regime for  $V_g < -10 \text{ V}$ , albeit with a small normal mode splitting: in this limit, highlighted by the dashed rectangle in Fig. 2b, it is not possible to directly measure the cavity line broadening (see Supplementary Information). As a finite electron density  $n_e$  is introduced by increasing  $V_g$  to  $-10 \text{ V}$ , a new absorption resonance (shaded blue curve), which is red-detuned by  $\sim 25 \text{ meV}$  from the bare exciton resonance, emerges (Fig. 2d). At the same time, the exciton line blueshifts and broadens, thereby ensuring that the coupling to the cavity mode is in the perturbative limit. For  $V_g = 0 \text{ V}$ , the exciton resonance sharply shifts to higher energies as the lower-energy resonance becomes prominent (Fig. 2e). Further increase in  $V_g$  leads to an increasing energy of the redshifted resonance and an indiscernible exciton feature (Fig. 2f). We observe that for  $V_g > 20 \text{ V}$ , the MoSe<sub>2</sub> monolayer-induced cavity line broadening exhibits a spectrally flat blue tail in absorption (Fig. 2g). Since the cavity line-broadening (Fig. 2b) and line-shift (Fig. 2c) data are connected by Kramers–Kronig relations, we mainly refer to line broadening in the following discussion. We also remark that in our experiments we monitor only optical resonances associated with the so-called A-exciton manifold<sup>26</sup>.

We note that TMD monolayer PL at low  $n_e$  is known to exhibit a sharp peak that is typically associated with trion radiative recombination<sup>26</sup>: this identification may be justified by the fact that photo-excited carriers predominantly relax to the lowest energy molecular (trion) state, which in turn decays by spontaneous emission to an excited state of the 2DES. We observe that in Fig. 2e the PL line (green curve) is only slightly redshifted with respect to the peak in absorption. In contrast, increasing  $V_g$  further results in a redshift of the PL peak while the low-energy absorption peak experiences a blueshift (Fig. 2f). Further increase in  $n_e$  results in a large splitting exceeding 40 meV between the absorption and PL peaks (Fig. 2g), suggesting that they are associated with different elementary optical excitations.

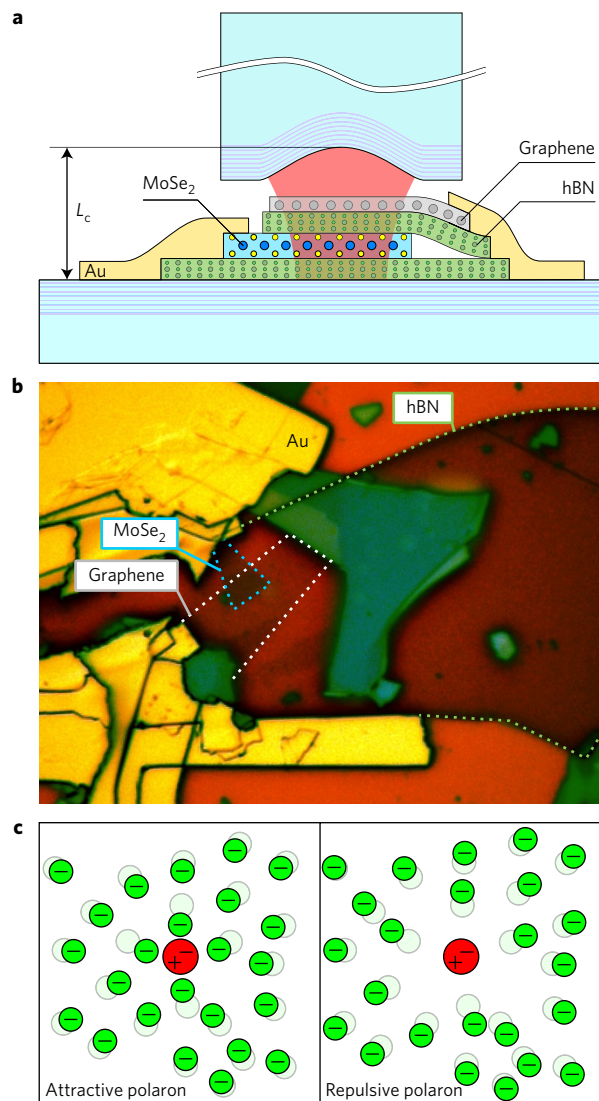


**Figure 1** | A MoSe<sub>2</sub>/hBN/graphene heterostructure in a fibre cavity. **a**, The sample consists of a  $3 \mu\text{m}$  by  $5 \mu\text{m}$  MoSe<sub>2</sub> monolayer sandwiched between 10-nm- and 110-nm-thick hBN layers. A graphene layer on top completes the heterostructure that allows for controlling the electron density in the MoSe<sub>2</sub> monolayer by gating. The heterostructure is placed on top of a flat dielectric mirror (DBR). The thicknesses of the hBN layers are chosen to ensure that the MoSe<sub>2</sub> monolayer is at an antinode and the graphene layer is at a node of the cavity formed by the bottom dielectric mirror and the top fibre mirror. The finesse of the cavity is  $\sim 200$ ; the cavity length can be tuned from  $1.9 \mu\text{m}$  to  $15 \mu\text{m}$ . **b**, The optical microscope image of the heterostructure where the overlap between the MoSe<sub>2</sub> monolayer and the top graphene layer is identified. **c**, Due to exciton–electron interactions, the exciton is surrounded by an electron screening cloud that leads to the formation of an attractive polaron (left panel). For a repulsive polaron the electrons are pushed away from the exciton leading to a higher-energy metastable excitation (right panel).

We identify the emerging lower-energy resonance in absorption for  $V_g \geq -10 \text{ V}$  as stemming from attractive exciton-polarons (Fig. 1c). The observation of substantial line broadening of the cavity mode indicates a sizable overlap between the ground state (with no optical or electronic excitation above the Fermi sea) and the optically excited state. These observations in turn render it unlikely that the observed features are associated with direct optical excitation of a trion. In contrast to the trion an attractive polaron has a finite amplitude for having no electron–hole pair excitation

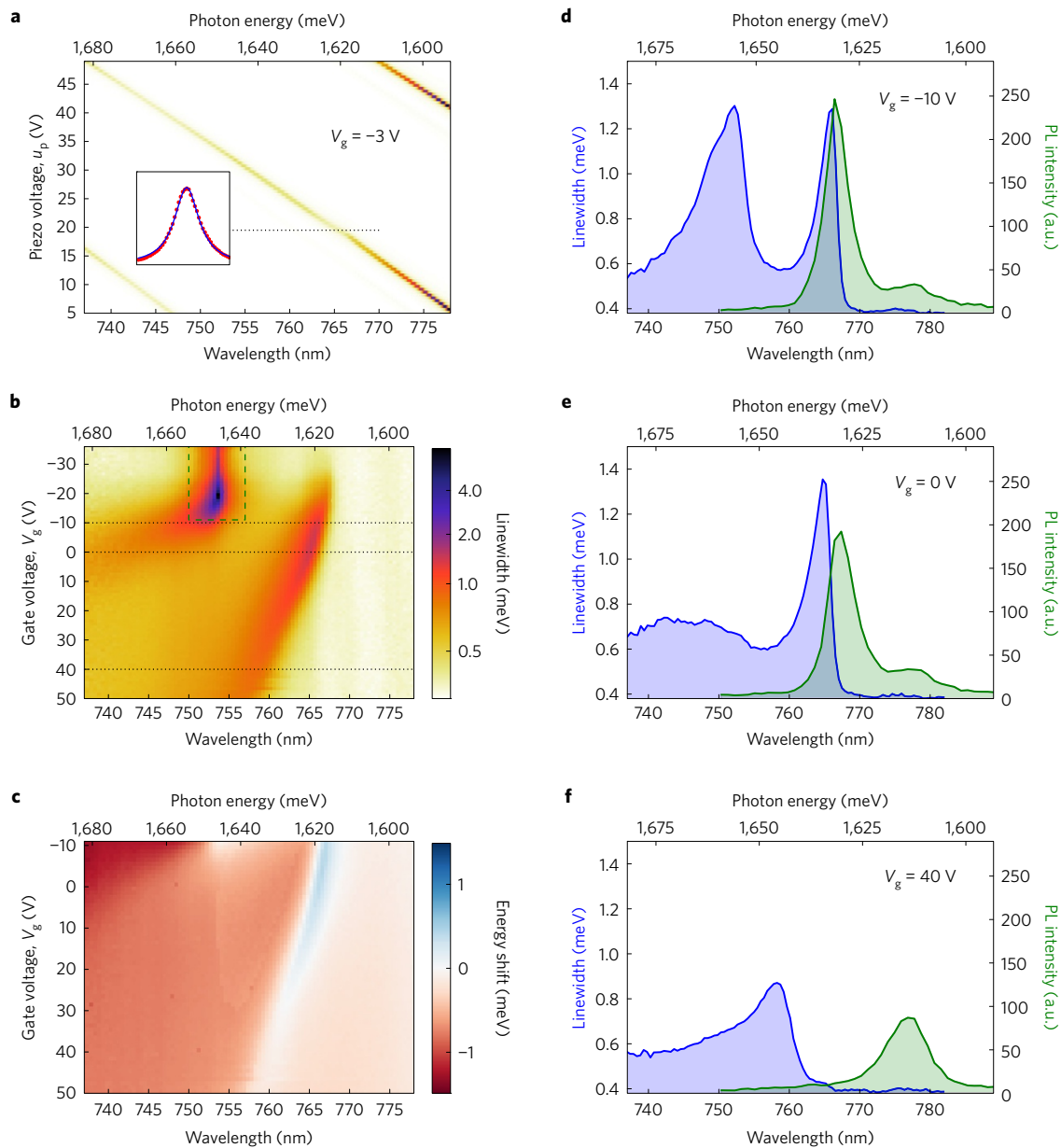


**Figure 2 | Cavity spectroscopy of the interacting exciton-electron system in the weak-coupling regime.** **a**, The white-light transmission spectrum of the fibre cavity incorporating the MoSe<sub>2</sub>/hBN/graphene heterostructure, as a function of the piezo voltage (vertical scale) that is varied to tune the cavity frequency. Since the bare cavity linewidth of 0.38 meV is much smaller than all other energy scales, cavity transmission allows for identifying the linear optical response of the heterostructure: whenever the cavity mode is at a frequency absorbed by the MoSe<sub>2</sub> flake, its linewidth increases. Consequently, the MoSe<sub>2</sub> absorption spectrum can be measured as a frequency-dependent broadening of the cavity. The inset shows the cavity transmission at  $V_g = -3$  V and  $u_p = 20$  V fitted with a Lorentzian curve. **b**, The MoSe<sub>2</sub> absorption spectrum determined by measuring the enhancement of the cavity linewidth for each cavity frequency (horizontal axis) and gate voltage (vertical axis). When the Fermi energy is below the conduction band minimum ( $V_g \leq -26$  V), absorption is observed only at the bare exciton frequency. As electrons are introduced, the exciton resonance experiences a sharp blueshift together with broadening. Concurrently, there is a new resonance emerging  $\sim 25$  meV below the bare exciton energy. These features are identified as the repulsive and attractive exciton-polaron resonances. For  $V_g < -10$  V, the exciton and the cavity mode are in the strong-coupling regime (the region highlighted using the dashed rectangle) and it is not possible to directly extract the imaginary part of the MoSe<sub>2</sub> linear susceptibility: in this regime, we measure and plot the linewidth of the cavity-like polariton. **c**, The measured real part of the susceptibility of the MoSe<sub>2</sub> flake as a function of the cavity frequency (horizontal axis) and the gate voltage (vertical axis). The data presented here are connected to the absorption data of **b** via Kramers-Kronig relations. In the absence of the MoSe<sub>2</sub> flake, there is an expected change of the cavity resonance (peak in the spectrum of the transmitted light) with changing piezo voltage. In the presence of MoSe<sub>2</sub>, the index of refraction seen by the photons is modified due to the real part of the MoSe<sub>2</sub> susceptibility, thereby modifying the effective cavity length and leading to a shift of the cavity resonance wavelength as compared with what we would have obtained in the absence of MoSe<sub>2</sub>. **d**, Line-cut through the cavity line-broadening data (blue shaded curve) for  $V_g = -10$  V ( $E_F = 5$  meV): both repulsive and attractive polaron features are visible. The trion and attractive polaron energies are comparable for this  $V_g$ . The PL data are shown in green. **e**, Line-cut through the cavity line-broadening data for  $V_g = 0$  V ( $E_F = 13$  meV): the line-broadening/absorption data are dominated by the attractive polaron that is now blueshifted with respect to the trion PL. **f**, Line-cut through the cavity line-broadening data for  $V_g = 40$  V: the PL and absorption peaks are separated from each other by 40 meV suggesting that PL and absorption data stem from different quasiparticles, namely the trion and the attractive polaron, respectively.

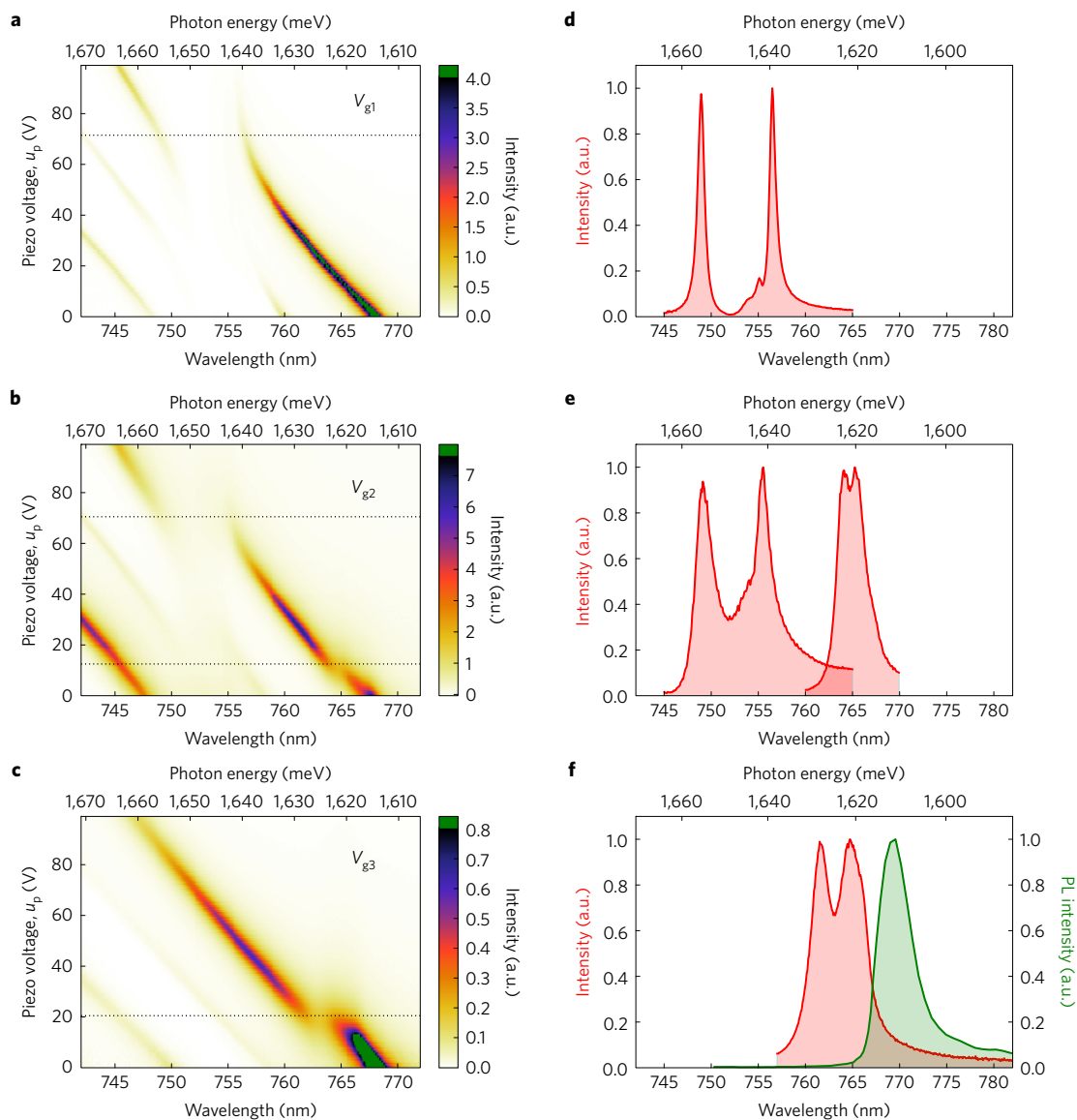


**Figure 3 | Cavity spectroscopy of the interacting exciton-electron system in the strong-coupling regime.** **a**, The white-light transmission spectrum as a function of the piezo voltage (vertical scale) for an average cavity length of  $1.9\ \mu\text{m}$ . Due to enhanced cavity electric field, the interaction between the cavity mode and  $\text{MoSe}_2$  resonances is directly observed in cavity transmission spectra as anticrossings associated with polariton formation. For gate voltages where the  $\text{MoSe}_2$  monolayer is devoid of electrons ( $V_{g1}$ ) the spectrum shows a prominent anticrossing with a normal mode splitting of  $16\ \text{meV}$ . The elementary optical excitations in this regime are bare exciton-polaritons without any polaron effect. **b**, White-light transmission spectrum for  $V_g = V_{g2} = -5\ \text{V}$ , showing two anticrossings associated with the formation of repulsive and attractive polaron-polaritons. The observation of anticrossings for both lower- and higher-energy resonances proves that these originate from Fermi polarons with a large quasiparticle weight. **c**, White-light spectrum for a higher gate voltage ( $V_{g3}$ ), where only the attractive polaron exhibits non-perturbative coupling to the cavity mode. **d**, Line-cut through the data in **a** for the piezo voltage  $u_p = 57\ \text{V}$  shows the transmission spectrum (red curve) at the resonance of the cavity with the exciton. **e**, Line-cut through the data in **b** for the piezo voltage  $u_p = 10\ \text{V}$  respectively  $u_p = 69\ \text{V}$ . **f**, Line-cut through the data in **c** for  $u_p = 25\ \text{V}$ , corresponding to the case where the cavity mode is resonant with the attractive polaron resonance. The PL spectrum in the strong-coupling regime is also plotted (green shaded curve).

across the Fermi surface ensuring a sizable quasiparticle weight. The strong  $n_c$ -dependent blueshift of the exciton resonance in turn indicates that it should be identified as the repulsive polaron—a metastable excitation of the interacting exciton–2DES system<sup>3</sup>.

The most spectacular signature demonstrating the polaron nature of the absorption resonances is obtained in the strong-coupling regime of the interacting cavity–exciton–electron system, which is reached by decreasing the effective cavity length to  $\sim 1.9\ \mu\text{m}$ . Figure 3a–c shows the transmission spectrum as the cavity length is changed by  $\sim 100\ \text{nm}$  at three different gate voltages. The observation of normal mode splitting when the cavity mode is tuned into resonance with the lower-energy absorption resonance

(Fig. 3b,c) demonstrates the large overlap between the initial and final states of this optical transition, which in turn proves that the resonance is associated with the attractive exciton-polaron. In contrast, the trion transition should have vanishing overlap with the 2DES ground state and should not lead to strong coupling to the cavity (see Supplementary Fig. 1). We also emphasize that the PL spectrum, which we associate with trion emission, shows no normal mode splitting for the parameters that yield split attractive polaron-polariton peaks in transmission (Fig. 3f).

Figure 3d–f shows cross-sections through Fig. 3a–c. The simultaneous appearance of polaritons in both the repulsive and attractive polaron branches (Fig. 3e) indicates that our experiments make it

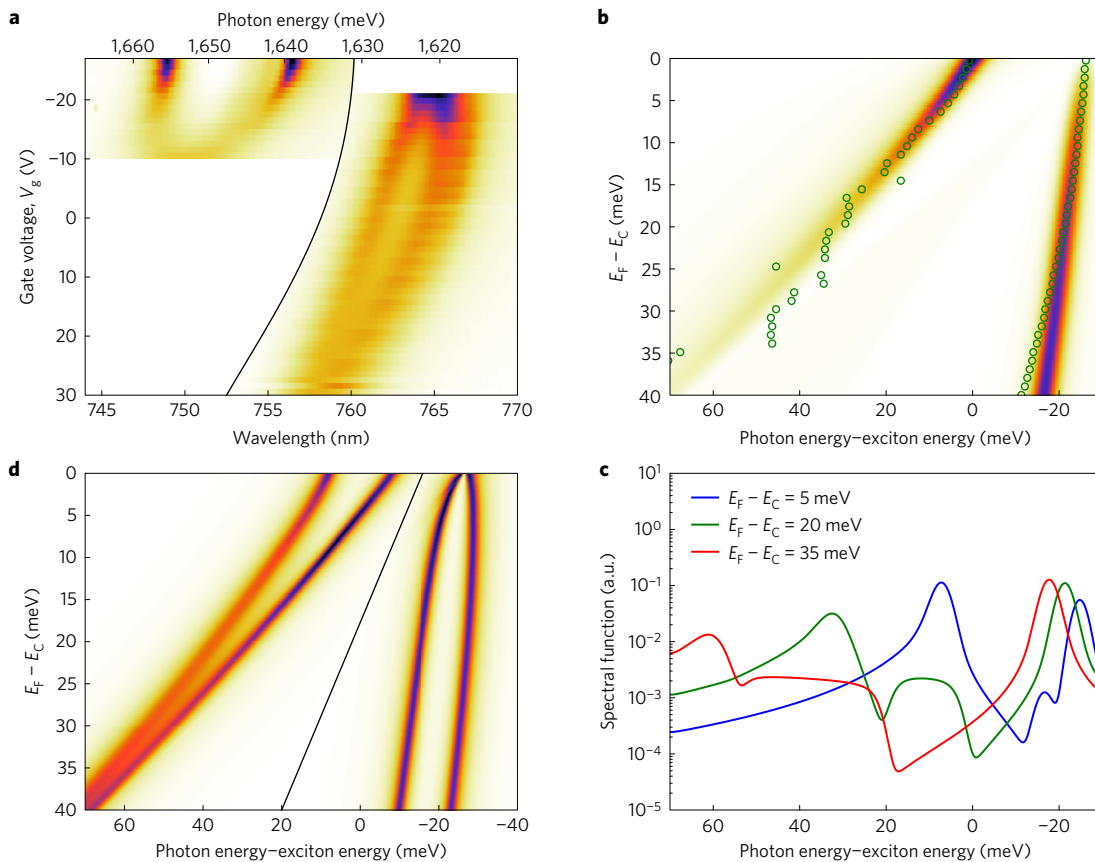


**Figure 4 | Competition between repulsive and attractive polaron resonances.** **a**, The white-light transmission spectrum of the fibre cavity incorporating the MoSe<sub>2</sub>/hBN/graphene heterostructure, as a function of the gate voltage (vertical scale) for two different settings of the cavity length: the left (right) part shows the transmission when the cavity is tuned on resonance with the repulsive (attractive) polaron. For each horizontal line, the cavity frequency is tuned so as to yield two polariton modes with equal peak amplitude. As  $V_g$  is increased, the oscillator strength transfer from the repulsive to attractive branch is clearly visible. While the normal mode splitting for the repulsive branch disappears for  $V_g \approx -10$  V, the collapse of the splitting takes place at  $V_g = 25$  V for the attractive branch. **b**, The spectral function calculated using the Chevy ansatz in the weak-coupling regime showing the attractive and repulsive polaron branches as a function of  $E_F$ . The centre frequencies of attractive and repulsive polaron resonances determined using differential reflection on a MoSe<sub>2</sub> monolayer are shown in green dots. The only fitting parameter for the calculations is  $\beta = 0.8$ . **c**, Line-cuts through the calculated spectral function for three different values of  $E_F - E_C$ . The use of logarithmic scale reveals the small weight of the trion + hole continuum. **d**, The spectral function calculated using the Chevy ansatz in the strong-coupling regime captures the oscillator strength transfer from the repulsive to attractive polaron depicted in **a** but fails to predict the collapse of the normal mode splitting with increasing electron density.

possible to study a new regime of polaron physics where an ultralight polariton impurity is dressed with electron-hole pair excitations. An exciting future direction motivated by our observations is the investigation of signatures of polaron formation on polariton transport.

The emergence of the lower-energy resonance and the gradual disappearance of the exciton resonance as  $n_e$  is increased has been previously predicted and identified as oscillator strength transfer from the exciton to trion<sup>7,21</sup>. To investigate how strong coupling alters the polaron formation and the associated oscillator strength transfer, we measured the normal mode splitting over a large range of  $V_g$ . Figure 4a shows, as a function of  $V_g$ , the transmission spectrum of the MoSe<sub>2</sub> monolayer when the bare cavity mode is in resonance with the repulsive polaron (left) or the attractive polaron. Increasing  $n_e$  results in decreasing (increasing) normal mode splitting for the repulsive (attractive) polaron. However, the maximum splitting for the attractive polaron obtained for  $V_g \approx -5$  V is less than half as big as that of the exciton obtained in the absence of a 2DEG. Further increase in  $V_g$ , or equivalently increase of  $n_e$ , results in diminishing normal mode splitting. In this limit of high  $n_e$ , the optical oscillator strength is distributed over a broad energy range of order  $E_F$ , thereby suppressing the coupling to the narrow cavity mode.

For theoretical modelling we use the truncated basis method (see Supplementary Information), in which the Hilbert space is

restricted to include at most a single electron-hole pair. This variational approach has been proved to be surprisingly accurate. In comparison with the diagrammatic Monte Carlo technique, it has been shown that, due to the destructive interference of higher order processes, both the polaron energies<sup>28</sup> and the quasiparticle weights<sup>29</sup> are accurately described by this method. We remark that electron-electron interactions can be neglected if we truncate the Hilbert space to just one electron-hole pair, justifying their exclusion from equation (1). Similar results have been obtained in the context of excitonic excitations in quantum wells, by using a T-matrix approach<sup>23</sup>. Our simple theoretical model captures the most important experimental observations in MoSe<sub>2</sub> and is consistent with the results obtained in other TMD materials such as WS<sub>2</sub> (ref. 19).

We present the theoretical results in the weak-coupling regime in Fig. 4b. The colour plot shows the theoretically calculated spectral function as a function of  $E_F$ . On top of the colour plot we overlaid the centre frequencies of attractive and repulsive polaron resonances (green dots) measured using differential reflection on a second MoSe<sub>2</sub> monolayer that is not embedded inside a fibre cavity structure (see Supplementary Information). There is only one free parameter in our model,  $\beta$ , which we choose  $\beta = 0.8E_F$ : this results in a blueshift of all resonances. Our model

captures the ‘repulsion’ of the high- and low-energy resonances observed in experiments quantitatively, further justifying their identification as the repulsive and attractive polaron resonances. We also correctly reproduce the quasiparticle weight transfer from the repulsive polaron to the attractive polaron (see Supplementary Fig. 1). Furthermore, we partially capture the broadening (and eventual disappearance) of the repulsive polaron branch. The broadening of the attractive polaron branch should emerge in an extended truncated basis approach that includes an extra electron–hole pair.

Our model also predicts a trion–hole continuum of very small weight. We identify this continuum as the feature of width  $\approx 2/3E_F$  that appears to the blue of the attractive polaron and blueshifts with increasing Fermi energy towards the repulsive polaron. Although this feature is very faint in Fig. 4b, it is clearly visible in the logarithmic-scale line-cuts in Fig. 4c. In the Supplementary Information we justify the identification of this feature as the trion–hole continuum and also explicitly calculate its quasiparticle weight. We notice that the weight of the trion–hole continuum remains smaller than that of the attractive polaron branch by at least an order of magnitude (see Supplementary Fig. 1), supporting our claim that the polariton formation cannot be associated with trions due to the small overlap between the trion and the 2DES ground state + one cavity photon. In contrast to the negatively charged trion, a Fermi polaron described by the Chevy ansatz corresponds to a neutral bosonic excitation, consisting of a Fermi-sea electron–hole pair bound to an exciton<sup>23</sup>.

Figure 4d shows the calculated spectral function in the strong-coupling regime. We see that the polaron peaks become sharper due to the coupling to the narrow cavity. We capture the decrease (increase) in the light–matter coupling for the attractive (repulsive) polarons as  $E_F$  increases. We also capture the repulsion of the attractive/repulsive polaron–polariton branches. However, our model does not predict the collapse of the attractive polaron strong coupling to the cavity, since this feature appears at large Fermi energies, where our approximations break down.

Our experiments establish strongly bound excitons in TMD monolayers, simultaneously embedded in a 2DES and a microcavity, as a new paradigm for quantum impurity and polaron physics. In stark contrast to prior work, we identify the optical excitations that are accessible in resonant spectroscopy as repulsive and attractive exciton polarons and polaron–polaritons, which are simultaneously present for Fermi energies that are smaller than the molecular (trion) binding energy. For  $E_F$  exceeding the conduction band spin–orbit coupling, TMD monolayers exhibit both intra- and inter-valley trions that are coupled by electron–hole exchange<sup>30</sup>: an interesting open question is whether the Berry curvature of the corresponding exchange coupled intra- and inter-valley attractive polarons leads to novel transport signatures. While we report the measurement of the spectral function of the interacting polariton–2DES system, we highlight that it is possible to directly measure the non-equilibrium response of the system in the time domain using ultrashort laser pump–probe spectroscopy in the regime  $E_F \leq 10$  meV. Finally, another interesting extension of our work would be the investigation of a Bose–polaron problem where an optically injected  $-K$  valley polariton impurity interacts with Bogoliubov excitations out of a polariton condensate in the  $+K$  valley.

## Methods

Methods, including statements of data availability and any associated accession codes and references, are available in the [online version of this paper](#).

Received 4 July 2016; accepted 4 October 2016;  
published online 31 October 2016

## References

- Massignan, P., Zaccanti, M. & Bruun, G. M. Polarons, dressed molecules and itinerant ferromagnetism in ultracold Fermi gases. *Rep. Prog. Phys.* **77**, 034401 (2014).
- Schirotzek, A., Wu, C.-H., Sommer, A. & Zwierlein, M. W. Observation of Fermi polarons in a tunable Fermi liquid of ultracold atoms. *Phys. Rev. Lett.* **102**, 230402 (2009).
- Schmidt, R., Enns, T., Pietilä, V. & Demler, E. Fermi polarons in two dimensions. *Phys. Rev. A* **85**, 021602 (2012).
- Kohstall, C. *et al.* Metastability and coherence of repulsive polarons in a strongly interacting Fermi mixture. *Nature* **485**, 615–618 (2012).
- Koschorreck, M. *et al.* Attractive and repulsive Fermi polarons in two dimensions. *Nature* **485**, 619–622 (2012).
- Carusotto, I. & Ciuti, C. Quantum fluids of light. *Rev. Mod. Phys.* **85**, 299–366 (2013).
- Esser, A., Zimmermann, R. & Runge, E. Theory of trion spectra in semiconductor nanostructures. *Phys. Status Solidi B* **227**, 317–330 (2001).
- Ganchev, B., Drummond, N., Aleiner, I. & Falko, V. Three-particle complexes in two-dimensional semiconductors. *Phys. Rev. Lett.* **114**, 107401 (2015).
- Xu, X., Yao, W., Xiao, D. & Heinz, T. Spin and pseudospins in layered transition metal dichalcogenides. *Nat. Phys.* **10**, 343–350 (2014).
- Liu, X. *et al.* Strong light–matter coupling in two-dimensional atomic crystals. *Nat. Photon.* **9**, 30–34 (2015).
- Dufferwiel, S. *et al.* Exciton–polaritons in van der Waals heterostructures embedded in tunable microcavities. *Nat. Commun.* **6**, 8579 (2015).
- Laussy, F. P., Kavokin, A. V. & Shelyk, I. A. Exciton–polariton mediated superconductivity. *Phys. Rev. Lett.* **104**, 106402 (2010).
- Cotlet, O., Zeytinoglu, S., Sigrist, M., Demler, E. & Imamoglu, A. M. C. Superconductivity and other collective phenomena in a hybrid Bose–Fermi mixture formed by a polariton condensate and an electron system in two dimensions. *Phys. Rev. B* **93**, 054510 (2016).
- Chernikov, A. *et al.* Exciton binding energy and nonhydrogenic Rydberg series in monolayer  $WS_2$ . *Phys. Rev. Lett.* **113**, 076802 (2014).
- Srivastava, A. & Imamoglu, A. Signatures of Bloch-band geometry on excitons: nonhydrogenic spectra in transition-metal dichalcogenides. *Phys. Rev. Lett.* **115**, 166802 (2015).
- Zhou, J., Shan, W.-Y., Yao, W. & Xiao, D. Berry phase modification to the energy spectrum of excitons. *Phys. Rev. Lett.* **115**, 166803 (2015).
- Wang, G. *et al.* Exciton states in monolayer  $MoSe_2$ : impact on interband transitions. *2D Mater.* **2**, 045005 (2015).
- Berkelbach, T. C., Hybertsen, M. S. & Reichman, D. R. Theory of neutral and charged excitons in monolayer transition metal dichalcogenides. *Phys. Rev. B* **88**, 045318 (2013).
- Chernikov, A. *et al.* Electrical tuning of exciton binding energies in monolayer  $WS_2$ . *Phys. Rev. Lett.* **115**, 126802 (2015).
- Rapaport, R., Cohen, E., Ron, A., Linder, E. & Pfeiffer, L. N. Negatively charged polaritons in a semiconductor microcavity. *Phys. Rev. B* **63**, 235310 (2001).
- Smolka, S. *et al.* Cavity quantum electrodynamics with many-body states of a two-dimensional electron gas. *Science* **346**, 332–335 (2014).
- Jacqmin, T. *et al.* Direct observation of Dirac cones and a flatband in a honeycomb lattice for polaritons. *Phys. Rev. Lett.* **112**, 116402 (2014).
- Suris, R. A. *Optical Properties of 2D Systems with Interacting Electrons* 111–124 (Springer Netherlands, 2003).
- Koudinov, A. V. *et al.* Suris tetrons: possible spectroscopic evidence for four-particle optical excitations of a two-dimensional electron gas. *Phys. Rev. Lett.* **112**, 147402 (2014).
- Duine, R. & MacDonald, A. Itinerant ferromagnetism in an ultracold atom Fermi gas. *Phys. Rev. Lett.* **95**, 230403 (2005).
- Ross, J. S. *et al.* Electrical control of neutral and charged excitons in a monolayer semiconductor. *Nat. Commun.* **4**, 1474 (2013).
- Besga, B. *et al.* Polariton boxes in a tunable fiber cavity. *Phys. Rev. Appl.* **3**, 014008 (2015).
- Combescot, R. & Giraud, S. Normal state of highly polarized Fermi gases: full many-body treatment. *Phys. Rev. Lett.* **101**, 050404 (2008).
- Vlietinck, J., Ryckebusch, J. & Van Houcke, K. Quasiparticle properties of an impurity in a Fermi gas. *Phys. Rev. B* **87**, 115133 (2013).
- Yu, H., Liu, G.-B., Gong, P., Xu, X. & Yao, W. Dirac cones and Dirac saddle points of bright excitons in monolayer transition metal dichalcogenides. *Nat. Commun.* **5**, 3876 (2014).

## Acknowledgements

J. Reichel, A. Kis and R. Schmidt have made invaluable contributions to the experimental and theoretical aspects of this work. The authors also acknowledge many insightful discussions with C. Ciuti, M. Combescot, M. Fleischhauer,

L. Glazman, M. Goldstein, F. Grusdt, D. Pimenov and J. von Delft. This work is supported by an ERC Advanced investigator grant (POLTDES), NCCR Quantum Science and Technology (NCCR QSIT), a research instrument of the Swiss National Science Foundation (SNSF), Harvard-MIT CUA, NSF Grant No. DMR-1308435, M. Rössler, the Walter Haefner Foundation and the ETH Foundation.

### Author contributions

M.S. and A.I. designed and supervised the experiment. M.S. carried out the measurements. P.B. fabricated the sample. T.F. and M.S. designed and assembled the cavity structure. A.S. and M.K. helped with the experiments. O.C., E.D. and A.I.

developed the theoretical model. O.C. carried out the calculations. M.S., O.C. and A.I. wrote the manuscript.

### Additional information

Supplementary information is available in the [online version of the paper](#). Reprints and permissions information is available online at [www.nature.com/reprints](http://www.nature.com/reprints). Correspondence and requests for materials should be addressed to M.S. or A.I.

### Competing financial interests

The authors declare no competing financial interests.

## Methods

The heterostructure studied in this work was assembled using the pickup technique<sup>31</sup>: flakes of the constituent materials are exfoliated onto separate substrates and sequentially picked up with a polycarbonate layer that finally deposits the complete heterostructure onto the target substrate. The target substrate in this case is a distributed Bragg reflector (DBR) ion beam sputtered onto a fused silica substrate. The DBR is designed to have a reflectivity of  $>99.3\%$  for the spectral range of 680–800 nm and an intensity maximum at the DBR surface. The graphene top gate and the MoSe<sub>2</sub> flake were contacted using metal gates consisting of a thin layer of titanium followed by a thicker layer of gold. To increase the chance of a good contact to the MoSe<sub>2</sub> flake, a parallel contact via a second graphene flake was made.

The top mirror is formed by a dimple with radius of curvature of 30  $\mu\text{m}$  shot into the fibre facet with a CO<sub>2</sub> laser. The geometry of the dimple was measured using interferometry. The fibre facet was coated with the same DBR as described above. All measurements are performed using a dipstick immersed in liquid helium. The sample can be moved in the ( $x$ - $y$ ) plane using nanopositioners. In addition, the cavity length is adjusted with a  $z$ -axis nanopositioner. Light from a (broadband) light-emitting diode covering the spectral range of interest is sent

through the fibre with the dimple and the transmitted light was collected by an aspheric lens. A second light-emitting diode emitting green light, which overlaps with a transmission window of the DBR mirrors, is used to locate the flake.

For PL measurements, a 532 nm laser is sent through the fibre. This wavelength is within a transmission window outside the stop band of the DBR. Therefore, PL excitation is efficient and only marginally changing with the cavity length. To extract the PL spectrum, the cavity emission spectrum is measured as a function of cavity length. For each cavity length, the area and the centre wavelength of the PL escaping through the cavity mode are measured. Plotting the area against the centre wavelength of the cavity mode yields the PL spectrum of the flake.

**Data availability.** The data that support the plots within this paper and other findings of this study are available from the corresponding author on request.

## References

31. Zomer, P. J., Guimares, M. H. D., Brant, J. C., Tombros, N. & van Wees, B. J. Fast pick up technique for high quality heterostructures of bilayer graphene and hexagonal boron nitride. *Appl. Phys. Lett.* **105**, 013101 (2014).